JOURNAL OF PROPULSION AND POWER
Vol. 20, No. 2, March–April 2004

Hypervelocity Fuel/Air Mixing in a Shcramjet Inlet

Jean P. Sislian* and Bernard Parent†
University of Toronto Institute for Aerospace Studies, Downsview, Ontario M3H 5T6, Canada

The mixing of fuel with air in the inlet of a shock-induced combustion ramjet (shcramjet) is presented. The study is limited to nonreacting hydrogen/air mixing in an external-compression inlet at a flight Mach number of 11 and at a dynamic pressure of 1400 psf (67,032 Pa), with use of an array of cantilevered ramp injectors. Results are obtained using the WARP code solving the Favre-averaged Navier–Stokes equations closed by the Wilcox $k\omega$ turbulence model and the Wilcox dilatational dissipation correction, discretized by the Yee–Roe flux-limited scheme. Because of the fuel being injected at a very high speed, fuel injection in the inlet is found to increase the thrust potential considerably, with a gain exceeding the losses by 40–120%. Losses due to skin friction are seen to play a significant role in the inlet, because they are estimated to make up as much as 50–70% of the thrust potential losses. The use of a turbulence model that can predict the wall shear stress accurately is, hence, crucial in assessing the losses accurately in a shcramjet inlet. Substituting the second inlet shock by a Prandtl–Meyer compression fan is encouraged because it decreases the thrust potential losses and reduces the risk of premature ignition by reducing the static temperature, while decreasing the mixing efficiency by a mere 6%. One approach that is observed to be successful at increasing the mixing efficiency in the inlet is alternating the injection angle along the injector array. The use of two injection angles of 9 and 16 deg is seen to result in a 32% increase in the mixing efficiency at the expense of a 14% increase in the losses when compared to a single injection angle of 10 deg. When alternating injection angles are used, the mixing efficiency reaches as much as 0.47 at the inlet exit.

Nomenclature

c	=	species mass fraction
C_f	=	skin-friction coefficient, $2\tau_w/\rho_\infty q_\infty^2$
D_{array}	=	injector array spacing
D_{fuel}	=	depth of the fuel jet
D_{inlet}	=	depth of the domain
$\mathcal{F}_{\text{pot}}$	=	thrust potential
$\mathcal{F}_{\text{pot ref}}$	=	reference thrust potential, normally calculated at the engine inlet
$\mathcal{F}_{\text{skin friction}}$	=	body force vector due to skin friction
H_{fuel}	=	height of the fuel jet
H_{inlet}	=	height of the inlet
k	=	turbulence kinetic energy
k_{div}	=	user-defined constant used in conjunction with the $k\omega$ model in WARP
L_{inj}	=	length of the injector
L_{inlet}	=	length of the inlet
M	=	Mach number
M_c	=	convective Mach number, $(q_1 - q_2)/(a_1 + a_2)$
$\dot{m}$	=	mass flow rate
$\dot{m}_{\text{air, engine}}$	=	mass flow rate of air in the engine
$\dot{m}_{\text{engine}}$	=	mass flow rate in the engine
P	=	pressure
Pr_t	=	turbulent Prandtl number
q	=	magnitude of the velocity vector
r	=	mesh dimension factor
Sc_t	=	turbulent Schmidt number
T	=	temperature
x, y, z	=	Cartesian coordinates
y^+	=	nondimensional wall distance, $(y/\mu)\sqrt{\rho\tau_w}$
η_m	=	mixing efficiency
θ_1	=	first-injector compression angle
θ_2	=	second-injector compression angle
μ	=	viscosity
ξ_{verge}	=	user-defined convergence criterion threshold
ρ	=	density
τ_w	=	wall shear stress
ϕ	=	equivalence ratio
ϕ_g	=	global equivalence ratio
φ_{verge}	=	user-defined streamwise ellipticity sensor

Subscripts

b	=	station of interest
c	=	engine outlet
t	=	turbulent
w	=	wall
∞	=	freestream

Superscripts

R	=	reacting
S	=	stoichiometric
$\star$	=	sum of the molecular and turbulent counterparts
$\circ$	=	stagnation

Received 31 July 2002; revision received 29 August 2003; accepted for publication 10 September 2003.

*Professor, Department of Aerospace Science and Engineering; sislian@caius.utias.utoronto.ca. Associate Fellow AIAA.

†Graduate Student, Department of Aerospace Science and Engineering; currently Research Associate, Department of Aerospace Engineering, Seoul National University, Seoul 151-744, Republic of Korea; bernard@snu.ac.kr. Student Member AIAA.

Introduction

FIRST proposed by Roy,[1] an alternate hypersonic propulsion concept that aims at increasing the fuel efficiency and thrust of the scramjet is the oblique detonation wave ramjet, also referred to as the shock-induced combustion ramjet (shcramjet).[2–4] The massive combustion chamber of the scramjet is avoided by burning the fuel/air mixture through a thin detonation wave, with the fuel injected in the inlet near the leading edge of the vehicle (Fig. 1). This reduces the weight of the engine and takes full advantage of the typically long inlets found at hypervelocities.

Preliminary predictions of the performance of detonation wave ramjets were performed through simplified one-dimensional analyses (Sargeant and Gross[5] or Dunlap et al.[6]). More detailed analytical models ensued by Townend,[7] Morrison,[8,9] and Ostrander et al.[10] to assess the on-design and even off-design performance of the flight vehicle. Inviscid simulations of planar and axisymmetric shcramjets

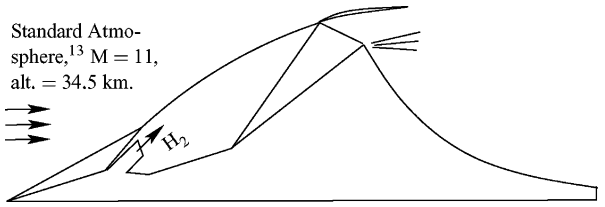

Fig. 1 External compression shcramjet schematic.

followed later by Sislian and Atamanchuk[2] and Atamanchuk et al.[11] using numerical methods based on exact and approximate Riemann solvers also including the nonequilibrium chemical kinetics equations for hydrogen/air combustion (Dudebout et al.[12]). The results obtained through the numerical studies confirm the encouraging performance of the shcramjet found in previous analytical work: 1) the shcramjet is seen to perform better than a scramjet at a flight Mach number above ~14 and 2) the shcramjet delivers a fuel specific impulse superior to that of a rocket up to a flight Mach number of ~22 (Ref. 12).

Besides neglecting viscous effects, all of the mentioned studies assume that the fuel and air are mixed in stoichiometric proportions before entering the engine and that no premature ignition occurs before the detonation wave. To the authors' knowledge, the only published work outlining the effect of incomplete fuel/air mixing on the shcramjet performance is Ref. 13, where an assessment is made of the impact of incomplete mixing on the net thrust by fixing a nonuniform equivalence ratio distribution at the inlet entrance. It is observed that an equivalence ratio distribution varying from $\phi \approx 2.4$ near the wall to $\phi \approx 0.02$ in the freestream decreases the fuel specific impulse by as much as 40% in the flight Mach number range $9 \leq M_{\text{flight}} \leq 24$. Because of the high sensitivity of the thrust of the shcramjet to incomplete fuel/air mixing, achieving adequate fuel/air mixing in the inlet while preventing premature ignition is one of the main technical challenges that needs to be resolved to establish the shcramjet as a viable hypersonic airbreathing flight vehicle.

There has been a recent interest in premixing the fuel with the air upstream of the combustor to improve the mixing and burning performance of scramjets. Vasilev et al.[14] numerically investigate the fuel/air mixing in a Mach 8 inlet by means of an injector structurally detached from the engine and placed well upstream of the inlet. At the inlet exit, a mixing completeness of as much as 0.6–0.7 is achieved without significant stagnation pressure losses. As a means to improve the efficiency of the heat release in scramjet combustors, Livingston et al.[15] and Owens et al.[16] consider liquid fuel preinjection in the inlet, upstream of the combustor. They experimentally investigate on the normal injection of liquid fuel JP-10 behind thin pylons in a Mach 1.6 and Mach 3.5 incoming airflow. The experimental results are representative of fuel injection in the inlet of a scramjet operating in the lower end of the hypersonic flight regime, where the high-enthalpy incoming airflow interacts with the lower speed fuel, hence, helping the process of liquid droplet breakup. The use of pylons to inject gaseous hydrocarbon in a Mach 6–8 scramjet inlet is further investigated numerically by Guoskov et al.,[17] who report a fuel-based mixing efficiency of 0.95–0.98 for a global equivalence ratio varying between 0.3 and 0.7, respectively. Both the experimental results by Livingston et al.[15] and Owens et al.[16] and the numerical results by Guoskov et al.[17] show that the pylons contribute significantly to lift the liquid from the injection surface, thus, avoiding fuel in the boundary layer and potential flashback.

In the present investigation, the fuel is injected through an array of cantilevered ramp injectors.[18–21] Specifically designed for fuel injection in shcramjet inlets, the cantilevered ramp injector generates axial vortices with a subsequent interface stretching comparable or superior to the one of ramp injectors,[18] while preventing the fuel from entering the hot boundary layer in the near field.[19] Furthermore, by injecting the fuel approximately in the same direction as the surrounding freestream flow direction, the cantilevered ramp injector ensures that the momentum of the fuel injected is recovered in the thrust balance, contrarily to the pylon injector, which injects the fuel perpendicular to the incoming air.

The main contribution of this paper consists of solving, for the first time in the literature, the important problem of fuel/air mixing in a shcramjet inlet using ramplike injectors. This study is limited to nonreacting hydrogen/air mixing in an external-compression inlet at a flight Mach number of 11 and at a dynamic pressure of 1400 psf (67,032 Pa), by use of an array of cantilevered ramp injectors. From earlier work by the authors on the effect of the fuel inflow conditions[19] and the injector geometry[20] on the mixing performance of the cantilevered ramp injector, a near-optimal baseline configuration is here considered in which 1) the convective Mach number is 1.2, 2) the global equivalence ratio approaches 1, 3) the sweeping angle is set to the minimum possible angle, and 4) the array spacing is set to the injector height. As indicated in Ref. 20, the sweeping angle corresponds to the angle between the sides of the injector and the incoming flow. A high sweeping angle would, hence, make the base of the injector wider than its tip, whereas a minimum sweeping angle (such as used herein) reduces the base of the injector to a minimal. The injector array is to be located between the first and second inlet compression processes, which can be both shocks, or a shock followed by a Prandtl–Meyer compression fan. For both cases, with use of the baseline injector configuration, the effect of fuel injection on the inlet performance is assessed. Then, the effort is focused on maximizing the mixing efficiency and thrust potential in the inlet by fine tuning the injector geometry and fuel inflow conditions. Particular attention is given to prevent the fuel/air mixture from entering the boundary layer, to avoid possible premature ignition.

The results are obtained using the WARP code,[19,22] in which the multispecies Favre-averaged Navier–Stokes equations closed by the Wilcox $k\omega$ turbulence model[23] are discretized by the Yee–Roe flux-limited method (see Ref. 24). To account for the compressibility effects occurring at high turbulent Mach number[19] the Wilcox dilatational dissipation correction[25] is used in conjunction with the $k\omega$ turbulence model. Convergence to steady state is achieved using block-implicit approximate factorization combined with local time stepping and the marching window acceleration technique.[22] The use of the marching window decreases the work by 10–20 times and the memory required by 5 times for the inlet cases shown herein and permits the solution of significantly finer meshes, hence, resulting in a decreased numerical error.

Problem Setup

The inlet cases considered are shown in Table 1. In each case, the letter C refers to a baseline cantilevered ramp injector geometry, as shown in Fig. 2, with the array spacing D_{array} set to 2 cm, the injection angle (θ_1, θ_2) set to 10 deg, the fuel jet depth D_{fuel} set to 1 cm, the fuel jet height H_{fuel} set to 1 cm, the injector length set to 7.5 cm, and the sweeping angle set to the minimum possible value, that is, −3.5 deg. The scale of the baseline injector is sufficiently small that the injector does not protrude beyond the first inlet shock. For the cases in which the letter C is immediately followed by w, the fuel inflow plane is replaced by a wall, and hence, no fuel is injected in the inlet. For cases containing the string F1, a shock–fan inlet configuration is in effect, as shown in Fig. 3, with the wedge angle set to 8 deg, followed by a compression surface with a

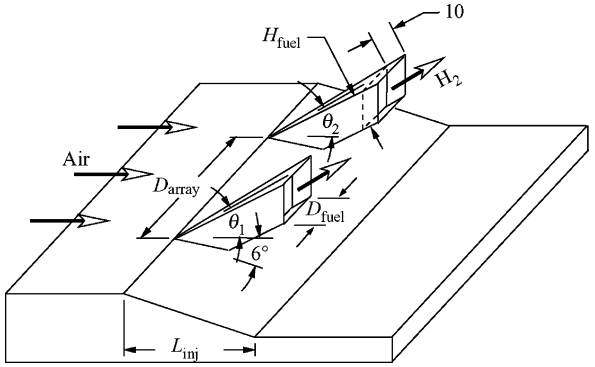

Fig. 2 Design of the cantilevered ramp injector for the inlet cases; all dimensions in millimeters unless otherwise specified.

Table 1 Test cases for the study of mixing optimization in a shcramjet inlet

Case	Inlet type	P_{H_2}, kPa	L_{inj}, cm	D_{array}, cm	D_{fuel}, cm	H_{fuel}, cm	θ_1, deg	θ_2, deg	r	Nodes, $\times 10^6$
S1_Cw	Shock–shock	——	7.5	2	1	1	10	10	1	3.4
S1_C1_g1	Shock–shock	9.6	7.5	2	1	1	10	10	0.67	1.1
S1_C1	Shock–shock	9.6	7.5	2	1	1	10	10	1	3.6
S1_C1_g3	Shock–shock	9.6	7.5	2	1	1	10	10	1.48	11.8
S1_C1d	Shock–shock	9.6	7.5	4	1	1	10	10	1	7
S1_C2	Shock–shock	4.8	7.5	2	1	1	10	10	1	3.6
S1_C1a5	Shock–shock	9.6	7.5	2	1	1	16	16	1	3.6
S1_C1a3	Shock–shock	9.6	7.5	2	1	1	16	9	1	7.1
S1_C1a3l1	Shock–shock	9.6	15.	2	1	1	16	9	1	7.2
S1_C1a3h1	Shock–shock	9.6	15.	2	0.5	2	16	9	1	9.9
F1_Cw	Shock–fan	——	7.5	2	1	1	10	10	1	3.8
F1_C1	Shock–fan	9.6	7.5	2	1	1	10	10	1	4.3
F1_C1d	Shock–fan	9.6	7.5	4	1	1	10	10	1	9
F1_C1a3h1	Shock–fan	9.6	15.	2	0.5	2	16	9	1	12.6

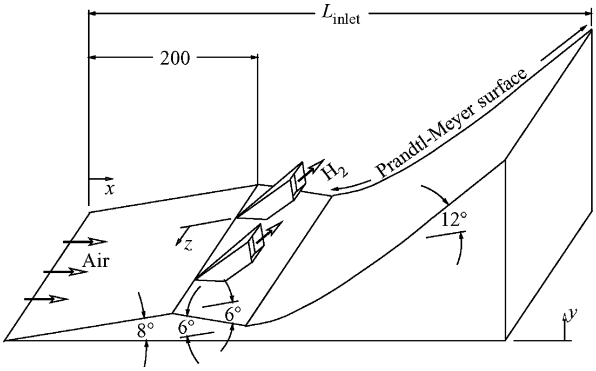

Fig. 3 Design of a shock–fan inlet, with the Prandtl–Meyer surface determined from initial Mach number of 7.575 and a focal point at $x = 1000$ mm and $y = 222$ mm; all dimensions in millimeters unless otherwise indicated.

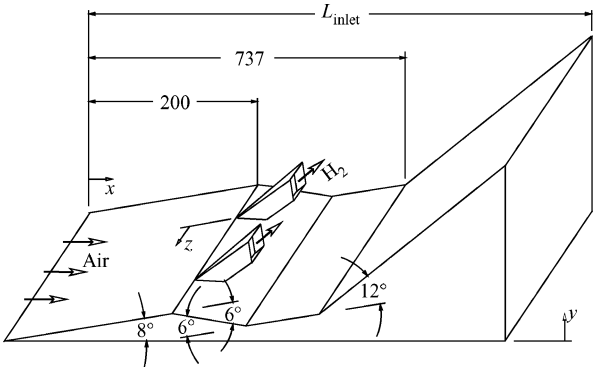

Fig. 4 Design of a shock–shock inlet; all dimensions in millimeters unless otherwise indicated.

flow turning angle of 12 deg and a focal point fixed to $x = 100$ cm, $y = 22.2$ cm. The y value of the focal point is determined from the y position of the first inlet shock at $x = 1$ m when a baseline injector geometry is used with no fuel injected, that is, case F1_Cw. Cases containing the string S1 are designed according to the shock–shock configuration shown in Fig. 4, with a first wedge angle of 8 deg followed by a second wedge angle of 12 deg located at $x = 73.7$ cm. The x position of the second inlet wedge is such that, for the baseline injector geometry with no fuel injected, that is, case S1_Cw, the two inlet shocks meet at $x = 1$ m, hence, resulting in an inlet length of 1 m. For the cases in which the letter C is followed by numeral 2, the hydrogen is injected at a pressure set approximately to that of the surrounding air, that is, 4800 Pa, whereas for the cases where letter C is followed by numeral 1, the fuel is injected at a pressure of 9600 Pa as a means to increase the global equivalence ratio. For all inlet cases, the fuel inflow stagnation temperature is set to 1200 K and the convective Mach number is set to a beneficially high value of 1.2, hence, resulting in a hydrogen inflow speed of 5257 m/s and in an inflow static temperature of 243 K. For a fuel inflow pressure specified to 4800 and 9600 Pa, the fuel inflow density corresponds to 0.00479 and 0.00958 kg/m^3, respectively. Cases with the letter d use an injector array spacing set to 4 cm instead of 2 cm. The string a5 refers to an injection angle of 16 deg, that is, $\theta_1 = \theta_2 = 16$ deg, instead of 10 deg, whereas the string a3 refers to an injection angle alternating between 9 and 16 deg, that is, $\theta_1 = 16$ deg and $\theta_2 = 9$ deg. The string l1 refers to a longer injector length $L_{inj} = 15$ cm, and the string h1 refers to an injector length $L_{inj} = 15$ cm and a fuel jet depth of $D_{fuel} = 0.5$ cm. The air inflow conditions for all cases correspond to those of the U.S. standard atmosphere[26] at an altitude of 34.5 km and at a flow Mach number of 11, resulting in a shcramjet flight dynamic pressure of 67,032 Pa. For those conditions, the air pressure, temperature, density, and speed entering the shcramjet inlet are found to correspond to 791 Pa, 237 K, 0.0115842 kg/m^3, and 3400 m/s, respectively.

Boundary Conditions

The temperature at the wall is set in all cases to 500 K. In the cases where no fuel is injected, the fuel inflow boundary condition is replaced by a fixed temperature wall. Second-order accurate symmetry planes are imposed for the front- and back-boundary planes, that is, at $z = 0$ and at $z = D_{array}/2$ for the cases with only one injection angle and at $z = 0$ and at $z = D_{array}$ for the cases with two injection angles. A short 10-mm-long runway is imposed to the fuel jet before being injected, to avoid a singularity in the turbulence and other flow properties at the start of the mixing layer. The left and top boundaries are set to supersonic inflow, with the right boundary set to supersonic outflow.

Performance Parameters

The air-based mixing efficiency η_m at the station of interest (denoted by subscript b) is defined as the ratio between the mass flux of oxygen that would react (if the flow temperature would be raised beyond the ignition point) by the mass flux of oxygen entering the engine:

$$\eta_m \equiv \int_b c_{O_2}^R \, d\dot{m} \Big/ 0.235 \times \dot{m}_{air,\,engine} \tag{1}$$

with $\dot{m}_{air,\,engine}$ determined as the product between the air inflow density, the air inflow speed, the height of the inlet, and the depth of the domain, that is, $\dot{m}_{air,\,engine} = 0.0115842$ kg/m^3 $\times$ 3400 m/s $\times$ $H_{inlet} \times D_{inlet}$. Note that the depth of the computational domain D_{inlet} corresponds to half the array spacing for the cases where $\theta_1 = \theta_2$ and to the array spacing for the other cases. The inlet length L_{inlet} and inlet height H_{inlet} correspond to the x and y positions at which the

Table 2 Tabulated performance parameters for the shcramjet inlet cases

Case	L_{inlet}, cm	H_{inlet}, cm	ϕ_g	η_m exit	$\mathcal{F}_{\text{pot}}$ gain, N · s/kg	$\mathcal{F}_{\text{pot}}$ loss, N · s/kg	$\mathcal{F}_{\text{pot}}$ exit, N · s/kg	$\mathcal{F}^x_{\text{skin friction}}$, N · s/kg
S1_Cw	100	22.3	0	0	0	80.2	−80.2	45.1
S1_C1_g1	108.4	26.7	0.813	0.30	129.8	67.9	61.8	40.6
S1_C1	108.2	26.5	0.819	0.31	131.4	68.6	62.9	41.5
S1_C1_g3	108.1	26.5	0.819	0.31	131.8	68.7	63.1	42.2
S1_C1d	101.4	23.2	0.473	0.30	75.1	71.5	3.6	43.5
S1_C2	105.4	24.9	0.441	0.31	68.7	72.8	−4.1	44.0
S1_C1a5	116.1	31.0	0.703	0.29	111.6	85.5	26.0	39.9
S1_C1a3	110.5	28.1	0.774	0.41	123.6	78.3	45.3	42.4
S1_C1a3l1	116.3	31.2	0.698	0.45	110.9	96.1	14.9	42.4
S1_C1a3h1	109.8	27.7	0.784	0.47	124.1	87.5	36.6	46.2
F1_Cw	100.	22.2	0	0	0	65.1	−65.1	48.9
F1_C1	107.9	26.9	0.807	0.30	129.5	57.9	71.6	42.8
F1_C1d	101.8	24.0	0.457	0.25	72.6	59.6	13.0	43.4
F1_C1a3h1	107.6	27.3	0.796	0.44	126.0	73.1	52.9	49.9

two inlet compression processes meet. The mass fraction of reacting oxygen, $c^R_{O_2}$, corresponds to

$$c^R_{O_2} = \min\left(c_{O_2}, c^S_{O_2} c_{H_2} \big/ c^S_{H_2}\right) \tag{2}$$

with the stoichiometric mass fraction of hydrogen $c^S_{H_2}$ equal to 0.02876 and the stoichiometric mass fraction of oxygen $c^S_{O_2}$ equal to 0.22824. Note that the mixing efficiency here assessed reflects the degree of bulk mixing, and not the degree of molecular mixing. To the authors' knowledge, it is not possible to assess accurately the degree of molecular mixing from numerical results obtained using a turbulence model because molecular mixing occurs at the smallest scales of turbulence, which are averaged in time and space by the turbulence model. Note that this limitation does not originate from the definition of the mixing efficiency [as pointed out in Eq. (1)], but rather from the $k\omega$ turbulence model used herein to obtain the results.

The thrust potential at a certain station, for example, station b, is defined as[20] the thrust that would be obtained if the flow would be reversibly expanded (without losses or gains) downstream of station b to a specified engine exit area:

$$\mathcal{F}_{\text{pot}} = -\mathcal{F}_{\text{pot, ref}} + \int_b \frac{\rho_c q_c^2 + P_c^\star}{\rho_c q_c} \frac{\mathrm{d}\dot{m}}{\dot{m}_{\text{air, engine}}} \tag{3}$$

where the properties assigned the subscript c are reversibly expanded from station b to an iteratively determined backpressure, which is such that the sum of the cross section of all streamtubes at station c corresponds to the engine inlet area.[20] The reference thrust potential, $\mathcal{F}_{\text{pot, ref}}$, is set to 3420.5 N · s/kg so that the thrust potential is zero at the inlet entrance. The normalized friction force on the body in the x direction, $\mathcal{F}^x_{\text{skin friction}}$ corresponds to the ratio between the skin-friction force experienced by the inlet in the x direction and the sum of the mass flow rate in the engine. This is done such that a comparison can be readily made between the thrust potential gains/losses and the losses due to friction.

Numerical Considerations

All inlet cases use a grid dimension factor $r = 1.0$, except for those marked with the strings g1 and g3, which refer to a mesh dimension factor $r = 0.674$ and $r = 1.484$, respectively. Note that the number of gridlines per meter is proportional to the mesh dimension factor r, so that the relative grid-induced error is expected to be similar for cases sharing the same mesh dimension factor. In Table 2, a comparison between cases S1_C1, S1_C1_g1, and S1_C1_g3 reveals that the mixing efficiency, the thrust potential gain, and the thrust potential losses vary by approximately 3, 3, and 1%, respectively, for a mesh dimension factor increased from 0.674 to 1.484. The small relative changes in the performance parameters is indicative of a small grid-induced error for case S1_C1. From the numerical error decay observed for a similar two-dimensional mixing problem, that is, the change of the properties observed over several grid levels, the numerical error is estimated to be 3–10% for the performance parameters presented in Table 2.

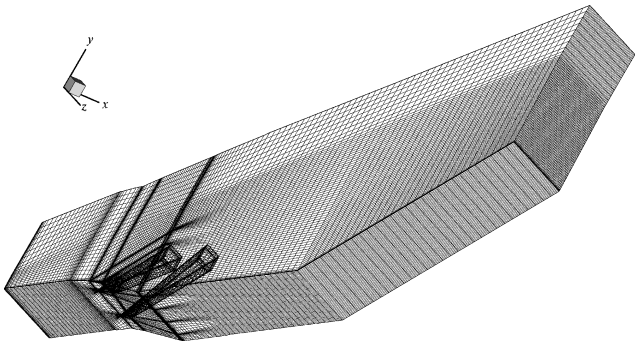

Fig. 5 Mesh used for case S1_C1a3l1, using a mesh dimension factor $r = 0.32$.

The mesh used for the inlet case F1_C1a3h1 using a mesh dimension factor of $r = 0.32$ is shown in Fig. 5. In the mixing region, the mesh is uniformly spaced in the streamwise coordinate x and in the spanwise coordinate z. Along y, the mesh exponentially grows from a specified wall node spacing of 10 μm to a uniform spacing in the mixing layer region. A wall node spacing of 10 μm in the mixing region is observed to result in a value of y^+ at the wall ranging typically from 1 to 3 for case F1_C1, with the maximum y^+ observed at the domain exit. Before the mixing region, the wall node spacing is set to 30 μm, which translates into a y^+ value ranging from 1 to 3 on the 8-deg wedge and injector surfaces.

The turbulent Prandtl number and the turbulent Schmidt number are set to 0.9 and 1.0, respectively, and are not altered in space. A value of k_{div} of 3×10^3 m^2/s^2 is used for all cases and is verified to be below the recommended[22] 1/10th of the maximum value of k present in the boundary layer. The maximum value of k in the boundary layer is verified for case F1_C1 to be typically 6×10^4 m^2/s^2, and reaches a minimum of 3×10^4 m^2/s^2 at $x = 65$ cm. No entropy correction term is used along with the Roe scheme for the inlet cases to avoid an excess of artificial dissipation, which would increase the grid-induced error. The standalone Roe scheme performs satisfactorily for a ramp injector mixing problem because the shock structure in the inviscid region of the flowfield is found to be unaffected by the inclusion of the entropy correction (see Ref. 19). Convergence is reached when $\xi \leq \xi_{\text{verge}}$ for all inner nodes, with the user-defined convergence criterion ξ_{verge} set to 4×10^2 1/s for all inlet cases, which has been shown to be sufficient for a similar problem.[19] Details on the definition of ξ can be found in Ref. 22. The streamwise ellipticity sensor threshold φ_{verge} is set to 7×10^4 1/s, and convergence to steady-state is reached typically in under 200 effective iterations by using the marching window acceleration technique.

Results and Discussion

Effect of Fuel Injection

In Table 2, the effect of fuel injection on the performance of a shock–shock inlet configuration is assessed by comparing case S1_Cw to case S1_C1. Similarly, a comparison between cases F1_Cw and F1_C1 reveals the impact of fuel injection on the performance of a shock–fan configuration. Note again that, in each inlet case, the strings C1 and Cw stand for a cantilevered ramp injector with and without fuel injected, respectively.

The first apparent effect of fuel injection is the increased length and height of the inlet, as shown by the parameters L_{inlet} and H_{inlet} in Table 2. This effect can be explained as follows. When no fuel is injected, a zone of low pressure is formed in the wake of the injector array and initiates an expansion fan that catches up with the first inlet shock (Fig. 6a). The shock strength and the shock angle are then reduced. By the injection of fuel, the formation of a low-pressure zone in the wake of the injector array is avoided, which results in a higher first inlet shock angle, as shown in Fig. 6b. A longer distance is then required for the second inlet shock (or the compression fan) to reach the first inlet shock, hence, resulting in an increase of approximately 8 and 19% in the inlet length and height, respectively, for either the shock–shock or the shock–fan inlet configurations.

A second marked effect of fuel injection on the performance of the inlet is the considerable gain in thrust potential due to the fuel being injected at a high speed (Fig. 7). As shown in Table 2, the gains in thrust potential are seen to be higher than the losses, with a gain/loss ratio of 1.9 and 2.2 for cases S1_C1 and F1_C1, respectively. Note that the small difference in thrust potential gain between case S1_C1 and case F1_C1 is due to the small difference in inlet height (and, therefore, of engine exit area) because the fuel inflow conditions and inflow cross-sectional area are identical for both configurations. Furthermore, note that the angle at which the fuel is injected does not influence the thrust potential gains. This might seem counterintuitive at first because one may expect fuel injection to contribute to the thrust of the vehicle only when injected parallel to the surrounding freestream direction. However, recall that the thrust potential corresponds, by definition, to the thrust of the engine obtained when the flow at one particular x station is reversibly expanded to the exit engine area with a velocity vector parallel to the surrounding freestream direction. Therefore, the thrust potential gains are independent of the injection angle because they are measured immediately downstream of the point of injection where the fuel has not yet undergone any irreversible process. However, note that fuel injected at a high injection angle is more likely to interact with the surrounding air inducing irreversibilities downstream of the point of injection, where thrust potential losses due to a high fuel injection angle would appear.

A third effect of fuel injection on the performance of the inlet is a net decrease in the thrust potential losses. For the shock–shock configuration, the thrust potential losses are seen to be decreased by 14%, whereas for the shock–fan configuration the decrease is slightly less pronounced at 11%. The decrease in thrust potential losses due to fuel injection is postulated to be partly due to the lack of a recirculation region inside the cantilevered ramp injector present when no fuel is injected and partly due to the reduction in skin friction in the mixing region. The reduction in skin friction due to fuel injection is found to be of 8% for the shock–shock configuration and of 12% for the shock–fan configuration (Table 2) and is due to a smaller wall shear stress in the high-pressure region after the second compression process. The reduction in shear stress in that region is attributed to the lower density of the flow at the wall because it is composed of a mixture of hydrogen and air, as opposed to pure air, as shown by the density contours at the domain exit in Fig. 8. Note that the wall shear stress for flow over a flat plate is directly proportional to the freestream density for constant freestream speed, Mach number, and Reynolds number, that is,

$$\tau_w \sim C_f \rho_\infty q_\infty^2$$

with C_f the skin-friction coefficient being a function of the flow Reynolds number and Mach number.

A fourth effect of fuel injection on the inlet performance is the decrease of the compression fan efficiency. Because of differences between the Mach number of the fuel jet and the adjacent air in the inlet, the compression process is not fully isentropic. Several small local shocks are observed throughout the compression fan (Fig. 6) caused by this difference in flow Mach number. These additional irreversible processes due to the presence of fuel are accounted for

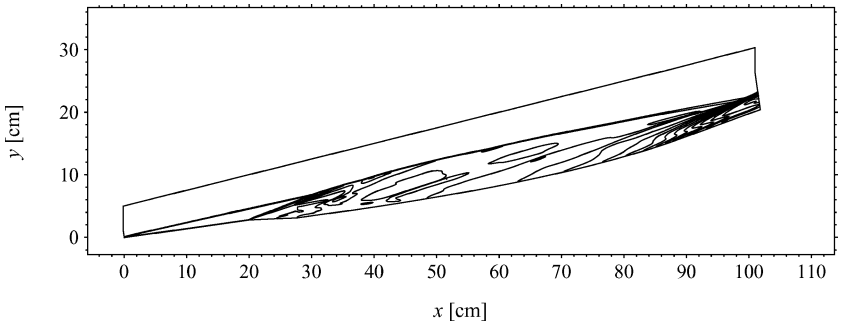

a) Inlet case F1_CW (without fuel injected)

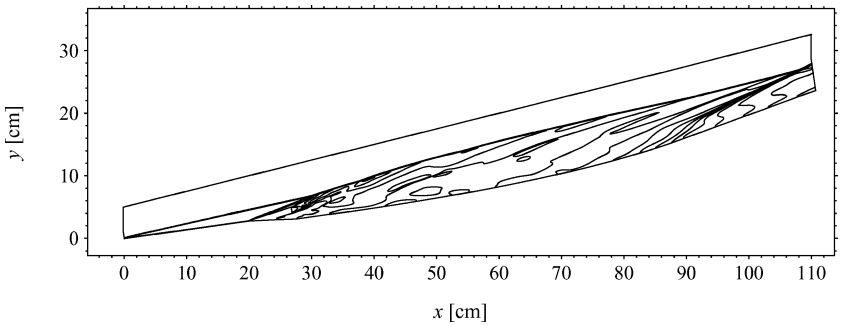

b) Inlet case F1_C1 (with fuel injected)

Fig. 6 Effective pressure contours of the baseline shock–fan inlet configuration in the plane $z = 0$ with and without fuel injected; 15 contours levels exponentially distributed between 800 and 32,000 Pa.

in the thrust potential losses, which, as can be seen in Table 2, show a smaller decrease for the shock–fan configuration, that is, a decrease of 11%, than for the shock–shock configuration, that is, a decrease of 14%, when fuel is injected. The reduction of the efficiency of the compression fan due to the presence of the fuel is further confirmed by the net 22% decrease in the mass flux averaged stagnation pressure between cases F1_Cw and F1_C1, as shown in Table 3.

Effect of Inlet Geometry

The replacement of the second inlet shock by a Prandtl–Meyer compression fan is expected to reduce the thrust potential losses considerably. In fact, on solving an inviscid two-shock inlet with a similar geometry as the shock–shock configuration but without the array of cantilevered ramp injectors, it is noticed that the thrust potential losses through the first shock are 12 N · s/kg and the thrust potential losses through the second shock are 30 N · s/kg. It might seem peculiar that the thrust potential losses are higher through the second inlet shock because the inlet is designed according to the Oswatitch condition with both oblique shocks at the same strength. It is reminded that this is due to the thrust potential not exhibiting a linear relationship with the stagnation pressure.[20] It follows that the use of a compression fan in lieu of the second inlet shock could reduce the thrust potential losses by as much as 30 N · s/kg. For the shock–fan inlet configuration, the compression fan is expected to be less efficient 1) due to the presence of an array of injectors in the inlet that creates some Mach number disturbances in the flow entering the compression fan and 2) due to the presence of a fuel at a different Mach number from the adjacent air. As already mentioned, variations in the flow Mach number are particularly detrimental to the performance of the compression fan due to the creation of small local shocks. Nonetheless, the use of a compression fan is seen to decrease the thrust potential losses other than those due to skin friction by 18.9 N · s/kg when no fuel is injected (hence, between

Table 3 Normalized[a] mass flux averaged flow properties at the inlet exit

	Mass flux averaged					
Case	ρ/ρ_∞	$P^\star/P^\star_\infty$	T/T_∞	q/q_∞	P°/P°_∞	T°/T°_∞
S1_Cw	8.58	35.5	4.15	0.917	0.233	0.983
S1_C1	7.82	34.1	3.65	0.929	0.219	0.874
F1_Cw	10.11	37.9	3.85	0.925	0.352	0.984
F1_C1	8.31	34.5	3.47	0.935	0.275	0.874

[a]Freestream properties correspond to $P^\star_\infty = 791$ Pa, $T_\infty = 237$ K, $q_\infty = 3400$ m/s, $\rho_\infty = 0.0115842$ kg/m^3, $P^\circ_\infty = 154.2$ MPa, and $T^\circ_\infty = 4856$ K.

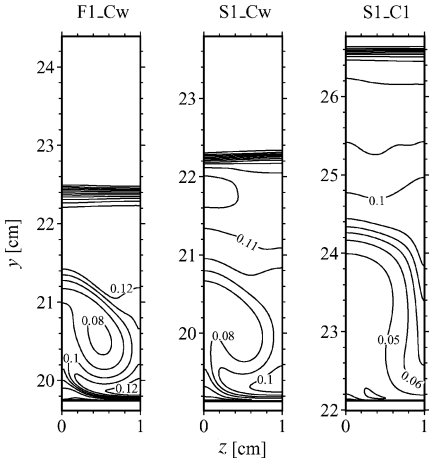

Fig. 8 Density contours in kilograms per cubic meter at the inlet exit for cases F1_Cw, S1_Cw, and S1_C1.

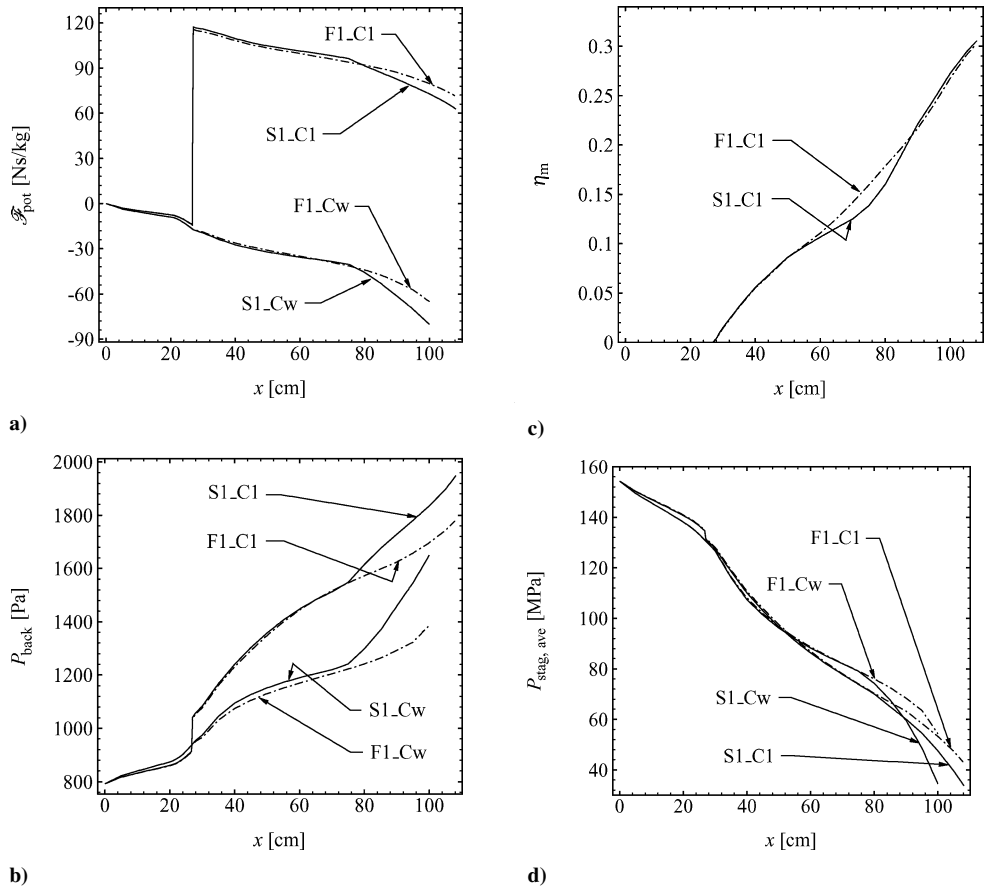

Fig. 7 Inlet cases S1_C1, S1_Cw, F1_C1, and F1_Cw comparison of a) thrust potential, b) backpressure, c) mixing efficiency, and d) mass flux averaged stagnation pressure.

cases F1_Cw and S1_Cw) and by 12.0 N · s/kg when fuel is injected (hence, between cases F1_C1 and S1_C1). As expected, the use of the compression fan is here seen to result in a decrease in the thrust potential losses short of the theoretical maximum of 30 N · s/kg, with a higher decrease in losses attainable when no fuel is injected.

Whereas the use of a compression fan in lieu of the second inlet shock is seen to decrease significantly the thrust potential losses related to the second compression process in the inlet, note that its use generally translates into a higher skin friction. This is attributed to the compression fan inducing a higher flow density (Fig. 8 and Table 3), which, as mentioned earlier, translates into a higher wall shear stress. Such is believed to be the cause of the 3–9% higher skin-friction force typically observed between the shock–fan configurations and the shock–shock inlet configurations. One notable exception to this trend, however, is in the case of a higher injector array spacing. As Table 2 attests, the skin-friction force is almost identical between the shock–shock and the shock–fan configurations at an array spacing of 4 cm, that is, between cases S1_C1d and F1_C1d. The fact that the skin-friction force is not altered between the two cases is peculiar because the shock–fan configuration is expected to exhibit a higher skin friction due to its higher flow density. The reason for this apparent contradiction is postulated to be the increased shear stress at the wall induced by axial vortices, which are known to be more pronounced for the shock–shock configuration.[27] The axial vortices are seen to entrain continuously a significant amount of the upper region of the boundary layer upward in the mixing region, effectively sustaining a high shear at the wall throughout the high-density mixing region. This effect can be seen through the temperature contours for the shock–shock inlet case S1_C1d in Fig. 9. The reason this effect is of less importance for the cases at an array spacing of 2 cm is due to the strength of the axial vortices being increased by a higher array spacing.[20]

Through a separate study of the effect of a shock and a compression fan on a freejet mixing layer,[27] it is observed that a compression fan results in a higher change in mixing efficiency growth for the same flow turning angle, despite clearly exhibiting weaker axial vortices induced through baroclinic torque. This was attributed to the higher density increase typical of an isentropic compression process. Note, however, that although the change in mixing efficiency growth is higher through the compression fan the resulting mixing efficiency at the domain exit was seen to be higher for the oblique shock configuration. This is a possible explanation to the observed slightly higher mixing efficiency for the shock–shock configurations than the shock–fan configurations, as seen in Table 2. There is, however, a second possible explanation for the observed higher mixing efficiency of the shock–shock inlet configuration. We note that the axial vortices generated by the compression process help the mixing in two ways in the inlet: first, by stretching the fuel/air

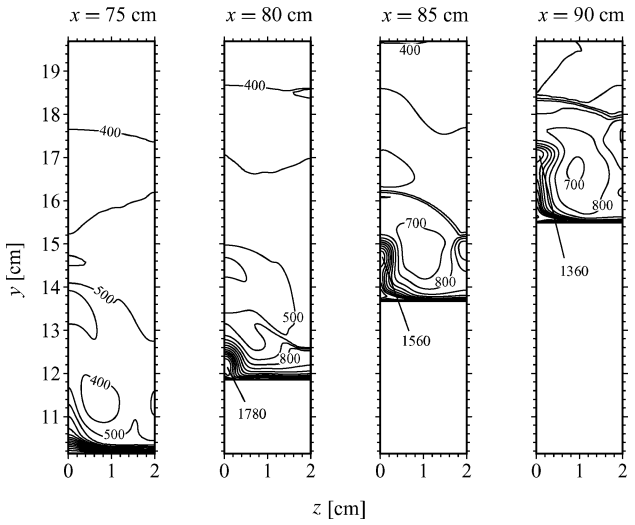

Fig. 9 Temperature contours in degrees Kelvin for several x stations downstream of the second inlet shock of case S1_C1d.

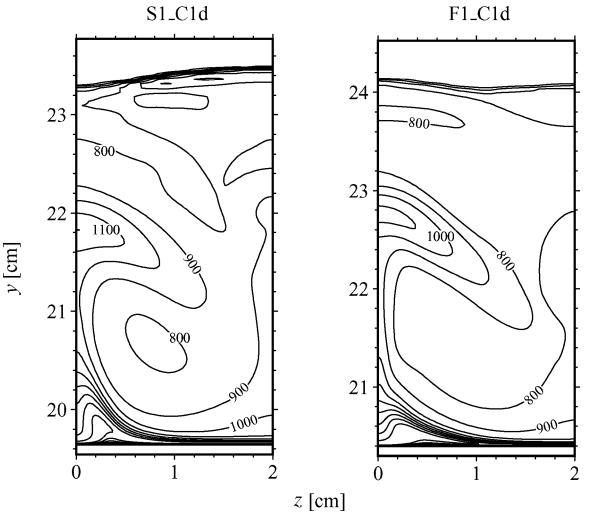

Fig. 10 Temperature contours in degrees Kelvin at the domain exit for cases S1_C1d and F1_C1d.

contact surface through axial vortices and, second, by enhancing the fuel penetration in the incoming air by entraining some air under the fuel jet. One important difference between the inlet cases and the cases presented in Ref. 27 is that, in the latter, the fuel jet is distanced sufficiently from the wall to prevent the mixing layer from reaching the wall boundary at any point downstream. Therefore, the greater penetration of the fuel in the incoming air due to stronger axial vortices does not enhance the mixing for the mixing configurations of Ref. 27. Such is not the case in the shcramjet inlet, where the fuel is seen to be relatively close to the wall and where good penetration induced by strong axial vortices help the mixing significantly by entraining some air under the fuel jet, hence, delaying the instant when the fuel/air interface reaches the wall boundary. Because the axial vortices induced by baroclinic torque are seen to be stronger in Ref. 27 when the mixing layer traverses an oblique shock than a compression fan, this could be a cause of the higher mixing efficiency exhibited by the shock–shock configurations compared to the shock–fan configurations, especially at increased array spacing.

A noteworthy feature of the shock–fan configurations is the reduced flow temperature increase through the second inlet compression process. A comparison between the temperature contours at the inlet exit of the shock–fan case F1_C1d and the shock–shock case S1_C1d in Fig. 10 reveals the static temperature of the shock–fan configuration to be, on average, approximately 70–80 K lower than the one of the shock–shock configuration. This is confirmed by the mass flux averaged temperature at the inlet exit between the baseline shock–shock and shock–fan configurations in Table 3. Besides decreasing the risk of premature ignition, a temperature reduction in the inlet improves the propulsive performance of the shcramjet[28] due to a more efficient heat release in the combustor. Nevertheless, note that the temperature decrease is less pronounced at a smaller array spacing, which is believed to be due to the higher global equivalence ratio affecting the efficiency of the compression fan.

Risk of Premature Ignition

A major concern when mixing in the inlet at hypersonic speeds is the high chance of premature ignition occurring in the hot boundary layer. By the distancing of the fuel jet from the wall at the point of injection, the cantilevered ramp injector design prevents the fuel from entering the boundary layer in the near-field mixing region. However, through the second inlet compression process, the flow is converged significantly in the y coordinate, which effectively decreases the height of the air buffer between the fuel and the wall by 3–4 times. Because the growth of the turbulent shear layer at a high convective Mach number is not altered significantly by the compression process,[27] it then follows that the air buffer separating the fuel from the wall gets completely eroded more rapidly in the high-pressure region. The convergence along y of the air buffer

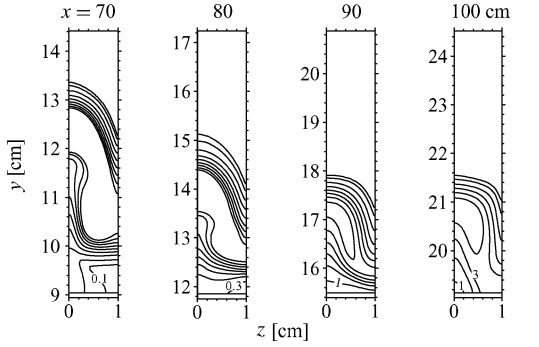

a) Inlet case S1_C1

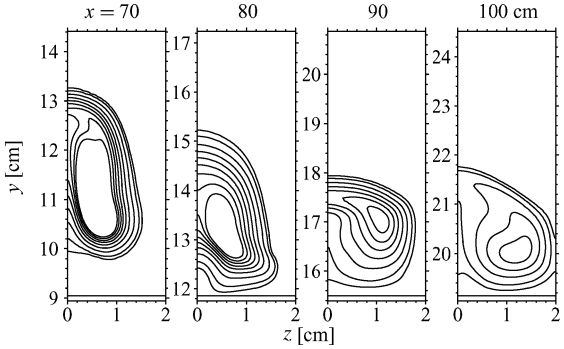

b) Inlet case S1_C1d

Fig. 11 Equivalence ratio contours of the shock–shock inlet configurations S1_C1 and S1_C1d; contours levels at $\phi = 0.1, 0.3, 1, 2, \ldots, 6, 7$.

caused by compression, hence, is seen to be the reason the fuel/air mixture enters the boundary layer between an x station of 80 and 90 cm for most of the inlet cases presented in Table 2. For the cases shown herein, the only way this could be avoided is by increasing the injector array spacing. Whereas increasing the array spacing does not prevent the air buffer between the fuel and the wall from being compressed by the compression process, a higher array spacing induces stronger axial vortices that entrain some air from in between the fuel jet to under the fuel jet, hence, preventing the air buffer from eroding completely in the high-pressure region (Fig. 11). Note however, that generating strong axial vortices is not sufficient to prevent fuel from entering the boundary layer. At the point where the axial vortices are created, there must also be a significant amount of pure air in between the fuel jets, which gets entrained under the fuel by the axial vortices. For the inlet cases at a low array spacing, there is no such region of air-only flow in between the fuel jets, and the axial vortices induced by baroclinic torque only serve the purpose of replacing the air buffer between the fuel and the wall by a combustible fuel/air mixture, further increasing the risk of premature ignition. Note that whereas the increased array spacing prevents, to some extent, fuel from entering the boundary layer, it generates axial vortices that entrain the hot air of the boundary layer in the mixing layer. Comparing the temperature contours of Fig. 10 to the equivalence ratio contours of Fig. 11, it is apparent that, for case S1_C1d, a fuel/air mixture is exposed to an above-ignition temperature in the plane $z = 0$ approximately 2 cm above the wall. The use of a high array spacing, hence, is seen not to prevent entirely the risk of premature ignition.

Mixing Efficiency Optimization

From Table 2, it is seen that a large portion of the thrust potential losses are due to skin friction, especially for the shock–fan configuration where the skin-friction force is seen to compose 68–75% of the losses for all shock–fan cases considered, with or without fuel injected. The remaining losses are estimated to be due mostly to flow irreversibilities associated with the first inlet shock. It follows that irreversibilities associated with the diffusion of hydrogen in the air are small by comparison and that a much higher amount of mixing occurring in the inlet is not expected to affect the thrust potential losses significantly. Furthermore, note that only small increases in the mixing efficiency in the inlet can result in very large thrust potential gains farther downstream in the combustor because the burning of a stoichiometric mixture of hydrogen and air is expected to induce a gain of as much as 400 N · s/kg for a shcramjet, that is, a fuel specific impulse gain of 1400 1/s (Ref. 12). Clearly, an additional 17% in the mixing efficiency could compensate for the entire thrust potential losses in the inlet of case F1_C1, for instance. Hence, in this subsection, we aim at increasing significantly the mixing efficiency with an improved injector geometry, while not being concerned about small increases in the losses.

The relatively low mixing efficiency obtained for the baseline shock–shock case S1_C1 ($\eta_m = 0.31$) and the baseline shock–fan fan F1_C1 ($\eta_m = 0.30$) is attributed mostly to the lack of penetration of the fuel in the incoming air. Although the hydrogen/air mixture is seen to be quite uniform in the bottom-half of the inlet exit (Fig. 11), no fuel is present in the upper-half. This clear lack of penetration is postulated to be due partly to the too short injector array distance, which reduces the air in between the fuel jets. Recall that a reduction in the amount of air in between the fuel jets prevents the axial vortices generated by the second inlet compression process from entraining air from above to under the fuel, which would result in better penetration. This is confirmed by comparing the hydrogen mass fraction profiles for a low and high array spacing in Fig. 11. Unfortunately, the use of an array spacing greater than the injector height decreases the mixing efficiency,[20] at least for a ramp injector mixing problem over a flat plate. This is confirmed for both the shock–shock and shock–fan inlet configurations because the mixing efficiency is not improved by an increased array spacing despite clearly showing better penetration.

A better fuel penetration can also be achieved through the use of a higher injection angle.[20] The impact of a higher injection angle is assessed by comparing case S1_C1 to case S1_C1a5, where the injection angle corresponds to 10 and 16 deg, respectively. Whereas the fuel-based mixing efficiency is seen to increase by 9% for the higher injection angle, the air-based mixing efficiency η_m decreases by 6%. This contradiction in trends between the air-based and the fuel-based mixing efficiencies originates from the 17% increase in inlet height for the higher injection angle. The increased height of the inlet is attributed to the stronger shock atop the injector array contributing to a stronger first inlet shock. The increased strength of the first inlet shock delays its meeting point with the second inlet shock, resulting in a higher inlet length and height. Therefore, although a greater amount of fuel is mixed with the air for the 16-deg injection angle case, this is not sufficient to increase the air-based mixing efficiency because the mass flow rate of oxygen entering the inlet also increases. This shows one of the difficulties of enhancing the mixing efficiency in an external compression inlet: The height of the inlet and, hence, the mass flow rate of oxygen entering the inlet are dependent on the mixing process itself. To increase the mixing efficiency, it follows that the inlet height must not be disturbed significantly by the increased fuel penetration.

One strategy investigated herein that is found to be successful at enhancing the fuel penetration without altering significantly the inlet height is the use of alternating injection angles, that is, giving θ_1 and θ_2 different values (Fig. 2). The high-angle injectors are responsible for the increased penetration, whereas the low-angle injectors help to reduce the flow blockage. A reduced flow blockage decreases the inlet height and also increases the mass flow rate of air in between injectors, hence, being particularly beneficial to the mixing efficiency. Shown in Table 2, an injection angle alternating between 9 and 16 deg (case S1_C1a3) is seen to result in a mixing efficiency increase of more than 32% when compared to a single injection angle of either 10 or 16 deg. Whereas the mixing efficiency is enhanced significantly, the associated thrust potential losses are seen to increase by a mere 9.7 N · s/kg. The success of an alternating injection angle configuration is partly attributed to the fuel jets emanating from the high-angle injectors distancing themselves from the fuel jets emanating from the low-angle injectors. This clearly results in two separate levels of fuel jets (Fig. 12) which translates

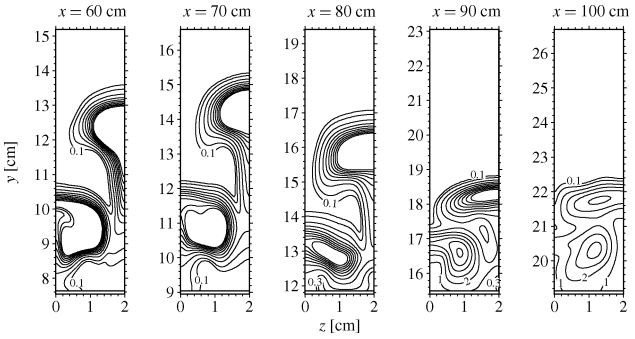

Fig. 12 Equivalence ratio contours of the shock–shock configuration S1_C1a3 with an injection angle alternating between 9 and 16 deg; contours levels at $\phi = 0.1, 0.3, 1, 2, \ldots, 6, 7, 8$.

into a much increased mass flow rate of air between the jets on each level. The axial vortices created by the compression process then increase the penetration by entraining the air from in between the fuel jets to under the jets, which eventually results in better mixing performance.

As a means to further enhance the mixing efficiency, we now consider a second fuel penetration strategy based on an increased injector length. If all of the other geometric parameters are kept constant, a longer injector translates into a greater distance between the fuel and the wall at injection and, hence, increases the mass flow rate of air under the fuel jet. Recall that an increase of air mass flow rate under the fuel is beneficial to the mixing efficiency by retarding the point at which the mixing layer reaches the wall.[20] Thus, we consider case S1_C1a3l1, which differs from case S1_C1a3 by a doubled injector length. Whereas the increased injector length provides better penetration, as is attested by the 10% increase in mixing efficiency in Table 2, the thrust potential losses are increased by as much as 17.8 N · s/kg. This relatively high increase in the losses is due to the greater flow blockage induced by the higher injectors. To reduce the amount of flow blockage while maintaining a high penetration, a new configuration is considered in which the injector length is doubled, while the depth of the fuel jets is reduced twofold. Furthermore, to maintain the same fuel inflow cross-sectional area, the fuel jet height is increased in the same proportion as the fuel jet depth is decreased. Such an inlet configuration is referred to as case S1_C1a3h1. It differs from case S1_C1a3 by a doubled injector length, a doubled fuel jet height, and a halved fuel jet depth, and it exhibits a mixing efficiency increase of 15% with an associated thrust potential loss increase of only 9.2 N · s/kg. Again, note that by reducing the thrust potential losses due to flow blockage, a better air-based mixing efficiency is obtained due to the reduced inlet height and increased oxygen mass flow rate in between injectors.

Conclusions

Because of the fuel being injected at a very high speed, fuel injection in the inlet is found to increase considerably the thrust potential, with a thrust potential gain typically exceeding the thrust potential loss by 40–120%. Another beneficial effect of fuel injection on the inlet performance is the observed decrease of approximately 10% in the skin-friction force. The decrease in skin-friction is attributed to fuel being present in the boundary layer after the second inlet compression process: The low density of hydrogen decreases the density of the boundary layer, thereby resulting in a reduced wall shear stress. However, the presence of fuel in the inlet is not all beneficial: Because the Mach number of the hydrogen stream is significantly lower than the Mach number of the airstream, the performance of the compression fan is reduced, with an associated increase in the thrust potential losses estimated to be of 8% for the shock–fan configurations.

Typically, it is estimated that 50–70% of the thrust potential losses in the inlet are due to skin friction. The large importance of the skin friction in the shcramjet inlet is seen to be partly due to the axial vortices generated by the second inlet compression process continuously entraining upward the upper part of the boundary layer, which results in a substantial thinning of the boundary layer, hence, increasing the wall shear stress.

The relatively low mixing efficiency of 0.30 obtained for the baseline inlet cases is attributed to the lack of adequate fuel penetration, partly due to the absence of a sufficient amount of air separating the fuel jets on entering the second inlet compression process. Furthermore, a major difficulty encountered while mixing in an external compression inlet is that the height of the inlet, and, hence, the amount of air entering the inlet, is strongly dependent on the fuel injection process. One novel approach that is shown herein to be successful at increasing the fuel penetration is alternating the injection angle from one injector to another. The use of alternating injection angles of 9 and 16 deg is seen to result in a 32% increase in the mixing efficiency and a 14% increase in the thrust potential losses when compared to injecting the fuel at a single injection angle of 10 deg. With use of an alternating injection angle, the mixing efficiency reaches 0.47 and 0.44 for the shock–shock and the shock–fan inlet configurations, respectively.

Premature ignition in the inlet is a high possibility for the baseline inlet configurations because a fuel/air mixture is seen to penetrate the hot boundary layer after the second inlet compression wave. One strategy that is shown here to prevent, to a large extent, the fuel from entering the boundary layer is the use of an increased injector array spacing. Unfortunately, although a higher array spacing prevents the fuel from entering the boundary layer, it results in stronger axial vortices that entrain the hot flow upward from the boundary layer to the mixing layer, which increases the risk of premature ignition in that region. The use of a shock–fan configuration reduces the risk of premature ignition by reducing the flow temperature in the mixing layer by as much as 80 K compared to the shock–shock configuration. Hence, the use of a Prandtl–Meyer compression surface in a shcramjet inlet is strongly recommended because it decreases the thrust potential losses and reduces the risk of premature ignition, while resulting in a small 6% diminution of the mixing efficiency for the optimal injector configuration considered.

Finally note that streamwise flow separation caused by shock wave–boundary-layer interactions did not occur in the inlet, either under the fuel at the point of injection or on the second inlet wedge. The lack of streamwise separation is attributed to the high resistance of the turbulent boundary layer to separate when the Mach number is high.

Acknowledgments

This work has been supported by the Natural Sciences and Engineering Research Council.

References

[1]Roy, M. M., "Moteurs thermiques," *Comptes Rendus de l'Académie des Sciences*, Vol. 222, No. 1, 1946.

[2]Sislian, J. P., and Atamanchuk, T. M., "Aerodynamic and Propulsive Performance of Hypersonic Detonation Wave Ramjets," *Proceedings of the 9th International Symposium on Air-breathing Engines*, AIAA, Washington, DC, 1989, pp. 1026–1035.

[3]Jones, J. S., Bangert, L. S., Garber, D. P., Huebner, L. D., McKinley, R. E., Jr., Sutton, K., Swanson, R. C., Jr., and Weinstein, L., "Research Opportunities in Advanced Aerospace Concepts," NASA TM 210547, Dec. 2000.

[4]Sislian, J. P., "Detonation Wave Ramjets," Scramjet Propulsion, edited by E. T. Curran and S. N. B. Murthy, Vol. 189 Progress in Aeronautics and Astronautics, AIAA, Reston, VA, 2001, Chap. 13, pp. 823–889.

[5]Sargeant, W. H., and Gross, R. A., "A Detonation Wave Hypersonic Ramjet," U.S. Air Force Office of Scientific Research, AFOSR, Technical Rept. 589, June 1959.

[6]Dunlap, R., Brehm, R. L., and Nicholls, J., "A Preliminary Study of the Application of Steady-State Detonation Combustion to a Reaction Engine," *Journal of Jet Propulsion*, Vol. 28, No. 6, 1978, pp. 451–456.

[7]Townend, L. H., "Detonation Ramjets for Hypersonic Aircraft," Royal Aircraft Establishment Technical Rept. 70218, Nov. 1970.

[8]Morrison, R. B., "Evaluation of the Oblique Detonation Wave Ramjet," NASA CR 145358, Jan. 1978.

[9]Morrison, R. B., "Oblique Detonation Wave Ramjet," NASA CR 159192, Jan. 1980.

[10]Ostrander, M., Hyde, J., Young, M., and Kissinger, R., "Standing Oblique Detonation Wave Engine Performance," AIAA Paper 87-2002, June 1987.

[11]Atamanchuk, T. M., Sislian, J. P., and Dudebout, R., "An Aerospace Plane as a Detonation Wave Ramjet/Airframe Integrated Waverider," AIAA Paper 92-5022, Dec. 1992.

[12]Dudebout, R., Sislian, J. P., and Oppitz, R., "Numerical Simulation of Hypersonic Shock-Induced Combustion Ramjets," *Journal of Propulsion and Power*, Vol. 14, No. 6, 1998, pp. 869–879.

[13]Sislian, J. P., Dudebout, R., Schumacher, J., Islam, M., and Redford, T., "Incomplete Mixing and Off-Design Effects on Shock-Induced Combustion Ramjet Performance," *Journal of Propulsion and Power*, Vol. 16, No. 1, 2000, pp. 41–48.

[14]Vasilev, V. I., Zokotenko, S. N., Krasheninnikov, S. J., and Stepanov, V. A., "Numerical Investigation of Mixing Augmentation behind Oblique Shock Waves," *AIAA Journal*, Vol. 32, No. 2, 1994, pp. 311–316.

[15]Livingston, T., Segal, C., Schindler, M., and Vinogradov, V. A., "Penetration and Spreading of Liquid Jets in an External–Internal Compression Inlet," *AIAA Journal*, Vol. 38, No. 6, 2000, pp. 989–994.

[16]Owens, M., Mullagiri, S., Segal, C., and Vinogradov, V. A., "Effects of Fuel Preinjection on Mixing in Mach 1.6 Airflow," *Journal of Propulsion and Power*, Vol. 17, No. 3, 2001, pp. 605–610.

[17]Guoskov, O. V., Kopchenov, V. I., Lomkov, K. E., and Vinogradov, V. A., "Numerical Research of Gaseous Fuel Preinjection in Hypersonic Three-Dimensional Inlet," *Journal of Propulsion and Power*, Vol. 17, No. 6, 2001, pp. 1162–1169.

[18]Sislian, J. P., and Schumacher, J., "A Comparative Study of Hypersonic Fuel/Air Mixing Enhancement by Ramp and Cantilevered Ramp Injectors," AIAA Paper 99-4873, Nov. 1999.

[19]Parent, B., Sislian, J. P., and Schumacher, J., "Numerical Investigation of the Turbulent Mixing Performance of a Cantilevered Ramp Injector," *AIAA Journal*, Vol. 40, No. 8, 2002, pp. 1559–1566.

[20]Parent, B., and Sislian, J. P., "Effect of Geometrical Parameters on the Mixing Performance of Cantilevered Ramp Injectors," *AIAA Journal*, Vol. 41, No. 3, 2003, pp. 448–456.

[21]Parent, B., and Sislian, J. P., "Impact of Axial Vortices on Mixing at a High Convective Mach Number," *AIAA Journal*, Vol. 41, No. 7, 2003, pp. 1386–1388.

[22]Parent, B., and Sislian, J. P., "The Use of Domain Decomposition in Accelerating the Convergence of Quasihyperbolic Systems," *Journal of Computational Physics*, Vol. 179, No. 1, 2002, pp. 140–169.

[23]Wilcox, D. C., "Reassessment of the Scale Determining Equation for Advanced Turbulence Models," *AIAA Journal*, Vol. 26, No. 11, 1988, pp. 1299–1310.

[24]Yee, H. C., Klopfer, G. H., and Montagné, J.-L., "High-Resolution Shock-Capturing Schemes for Inviscid and Viscous Hypersonic Flows," *Journal of Computational Physics*, Vol. 88, No. 1, 1990, pp. 31–61.

[25]Wilcox, D. C., "Dilatation-Dissipation Corrections for Advanced Turbulence Models," *AIAA Journal*, Vol. 30, No. 11, 1992, pp. 2639–2646.

[26]*The U.S. Standard Atmosphere (1962)*, U.S. Government Printing Office, Washington, DC, 1962.

[27]Parent, B., and Sislian, J. P., "Hypersonic Mixing Enhancement by Compression at a High Convective Mach Number," *AIAA Journal*, accepted 6 Oct. 2003 for publication.

[28]Sislian, J. P., Schirmer, H., Dudebout, R., and Schumacher, J., "Propulsive Performance of Hypersonic Oblique Detonation Wave and Shock-Induced Combustion Ramjets," *Journal of Propulsion and Power*, Vol. 17, No. 3, 2001, pp. 599–604.